ASME Journal of Engineering for Gas Turbines and Power
Online journal at:
https://asmedigitalcollection.asme.org/gasturbinespower

Joshua Bird
Department of Mechanical Engineering,
University of Bath,
Bath BA2 7AY, UK
e-mail: jb3315@bath.ac.uk

Patrick S. Keogh
Department of Mechanical Engineering,
University of Bath,
Bath BA2 7AY, UK
e-mail: p.s.keogh@bath.ac.uk

Carl M. Sangan
Department of Mechanical Engineering,
University of Bath,
Bath BA2 7AY, UK
e-mail: c.m.sangan@bath.ac.uk

Aaron A. Bowsher
Cross Manufacturing Ltd.,
Devizes SN10 2EU, UK
e-mail: aaron.bowsher@crossmanufacturing.com

Peter F. Crudgington
Cross Manufacturing Ltd.,
Devizes SN10 2EU, UK
e-mail: pete.crudgington@crossmanufacturing.com

James A. Scobie[1]
Department of Mechanical Engineering,
University of Bath,
Bath BA2 7AY, UK
e-mail: j.a.scobie@bath.ac.uk

Rotordynamics of a Single-Stage Brush Seal in Isolation: The Effects of Variable Stiffness and Back Plate Geometry

Brush seals control leakage around rotating components from areas of high to low pressure inside turbomachinery. They are known to contribute to the overall stability of gas turbines, therefore their dynamic behavior is of particular importance to engine designers. Despite this, limited research exists in the literature on the rotordynamic behavior of brush seals. This paper aims to experimentally characterize the leakage and rotordynamic performance of two seals with different bristle diameters tested with both conventional and pressure-relieved back plates with a slight interference. A dynamic test facility was utilized to study the dynamic characteristics of an isolated seal with changes in excitation frequency, rotational speed, and pressure drop. Seal leakage increased with bristle diameter and with the use of the pressure-relieved back plate but reduced with increasing rotational speed for all tests. The direct dynamic coefficients were shown to increase with pressure difference. The back plate geometry influenced the change in stiffness coefficient with rotational speed. The larger bristle diameter resulted in a stiffer seal, however, the damping coefficient reduced with the reduction in packing density. The insight provided by these results will help inform engine manufacturers on the suitability of implementing brush seals in future gas turbine designs.
[DOI: 10.1115/1.4066711]

1 Introduction

Gas turbines are used in the power generation and aviation industries. With the ever-growing demand for increased sustainability, there is a need to improve engine efficiency to ensure the continued development of both industries. The secondary air system (SAS) is used to bleed comparatively cool air from the compressor to the high-temperature turbine stages to seal bearing cavities and achieve higher turbine inlet temperatures, improving the overall efficiency of the engine. Seals are used throughout the SAS to control leakage flows between rotating and stationary components, as shown in Fig. 1.

Seals may be classified as either noncontacting or compliant. Noncontacting seals, such as the labyrinth seal, use a tight clearance to prevent flow. They usually allow shaft rotation in either direction and are inexpensive to manufacture. As tight clearances are required to minimize leakage flow, shaft rubs can cause wear, increasing leakage and reducing operational life. Another drawback of labyrinth seals is that they are known to create destabilizing forces that cause the rotor to eccentrically self-excite and move away from its stable center of rotation [2,3].

Compliant seals allow for eccentricities and variance in rotor clearance. This may be achieved through the use of flexible mechanical members or pressurized film-riding components [4,5]. Generally, compliant seals represent an improvement in tolerances for rubs and often a reduction in leakage [4].

First introduced by Ferguson [6], the brush seal is a mechanically compliant seal comprised of a bristle pack which is welded together and housed in between a front and back plate. The bristle pack is made up of densely packed, flexible, fine wire bristles often made of Haynes 25 that provide resistance to the flow. The back plate typically has a smaller clearance gap than the front plate, known as the fence height, denoted by h_f in Fig. 2. Additionally, the bristle pack bore can be machined to have a clearance or an interference fit, i, as shown in red in Fig. 2 (Color version online). In other words, i can be negative or positive, respectively [7,8]. The bristle pack is

Turbo Expo, June 24–28, 2024. GT2024.
[1]Corresponding author.
Manuscript received September 7, 2024; final manuscript received September 19, 2024; published online November 22, 2024. Editor: Jerzy T. Sawicki.

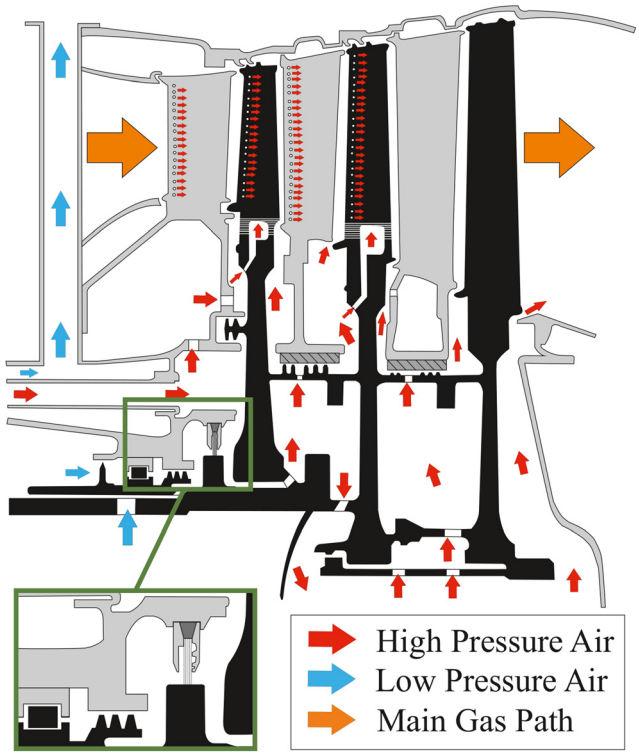

Fig. 1 Typical secondary air system [1]

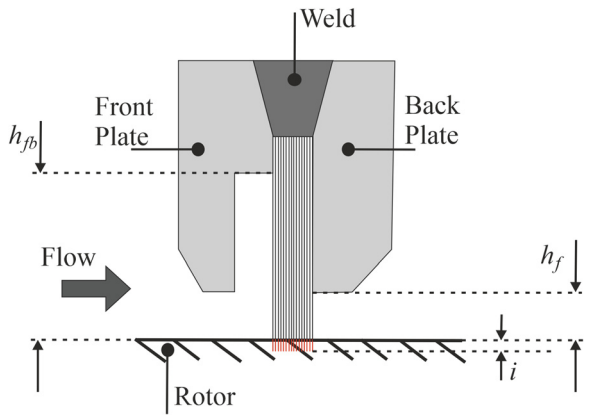

Fig. 2 Cross section of a brush seal

welded at a lay angle between 30 deg and 60 deg, which is optimized to minimize the contact forces between the bristles and the rotor [9].

The use of brush seals instead of labyrinth seals has led to improvements in gas turbine efficiency that have been well documented. For example, Hendricks et al. [10] replaced a forward facing labyrinth seals in a T-700 helicopter engine with a dual brush seal and tested up to 10 bar and 43,000 rpm. They demonstrated up to a 5% reduction in specific fuel consumption and 2.5 times reduction in leakage using brush seals instead of the labyrinth seal arrangement.

Kirk et al. [8] state that smaller diameter bristles will reduce leakage while larger diameters will have higher load capabilities and improved wear properties. Pekris et al. [11] and Proctor and Delgado [12] found that increased rotational speed reduced the leakage flow through the brush seal, which was attributed to the extended leakage path in the tangential direction and the reduced fence height with rotor growth. Additionally, Pekris et al. [11] found that using a back plate with an actively pressurized pocket decreased the leakage through the brush seal. This arrangement reduced hysteresis and so improved the compliant behavior of the bristle pack. However, this also correlated to an increase in torque and therefore would increase the wear rate of the seal.

Bowen et al. [1] studied the leakage and pressure field distribution through brush seals with conventional and pressure-relieved back plates. They found that introducing shaft rotation caused a reduction in leakage flow and an increase in static pressure on the back plate surface. Both effects were relatively insensitive to further increases in rotor speed. The use of the pressure-relieved back plate increased the static pressures on the back plate surface and increased the leakage flow. This was attributed to reduced compaction of the bristle pack and a steeper radial pressure gradient on the back plate surface.

There has been limited research regarding the rotordynamic stability of brush seals, however, several studies have focused on the dynamic behavior of compound seal arrangements featuring brush seals. Conner and Childs [13] measured the stiffness and damping coefficients for four brush seals in series up to a pressure ratio of 0.55. The bristles were made from Inconel X750 and assembled with a clearance between the tips and the rotor, these characteristics are no longer representative of modern brush seals. The study found that shaft rotation reduced the stiffness of the seals, but had limited effect on the damping coefficients. The reduction in direct stiffness with rotation was suggested to be caused by a fluid film developing between the bristle tips and the rotor. Increasing the pressure ratio increased both the direct stiffness and damping coefficients. The cross-coupled coefficients were found to be negligible.

A line-on-line brush seal in series with labyrinth seal fins was tested by Gaszner et al. [14] for two different arrangements. The mechanical stiffness introduced by the brush seal was shown to increase the overall stiffness. Additionally, the damping was generally higher when the brush seal was included rather than when the labyrinth seal was tested in isolation.

Pugachev and Deckner [15] studied the stiffness of three brush seals in series by integrating the circumferential pressure distribution measured upstream and downstream of each bristle pack. The brush seals were manufactured with a small clearance between the bristle tips and the rotor surface. They found that both the direct and cross-coupled stiffness increased with preswirl, and the coefficients were invariant with rotational speed.

Ha et al. [16] found that an increase in rotational speed decreased both the stiffness and damping coefficients of brush seals. They tested a seal in a superheated steam environment up to 0.6 bar pressure difference and found that the rotordynamic coefficients increased significantly when steam was introduced.

Delgado et al. [17] measured the energy dissipation characteristics of a shoed brush seal. Due to the interbristle frictional interactions, the seal behaved as a Coulomb damper rather than a viscous damper. The Reynolds equation was used to predict the stiffness characteristics of the shoed brush seal, which showed a decrease in direct stiffness with increased rotational speed [18].

There is a clear need to determine how different design parameters affect the stability characteristics of brush seals in order to understand how they will interact with a wider system of seals. This paper presents the dynamic behavior of four, state-of-the-art brush seal designs tested in isolation from any other components of an SAS. Two engine-representative back plates have been studied: a flat conventional plate and a pressure-relieved configuration. Additionally, two different bristle diameters have been tested with each back plate.

2 The Dynamic Test Facility and Salient Parameters

The dynamic test rig was designed and commissioned by Pedraza-Valle et al. [19]. A brief overview of the facility and operating conditions is given herein and a description of the four brush seal configurations is presented.

2.1 The Dynamic Test Rig. The facility is shown in Fig. 3 and was designed to study leakage and rotordynamic behavior of shaft seals when subject to external excitation [20].

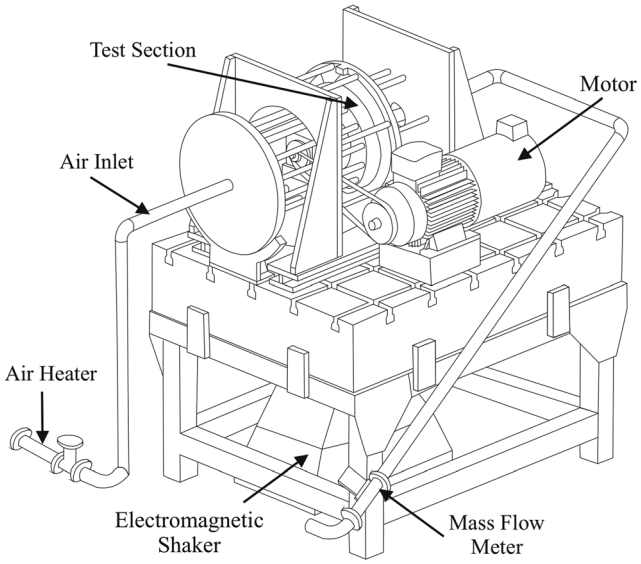

Fig. 3 Isometric view of the dynamic test facility [20]

The test section was raised on an iron bed plate to accommodate the electromagnetic shaker underneath used to excite the seal. The 254 mm (10 in) diameter shaft could rotate up to 15,000 rpm and was powered by a 15 kW motor. The shaft was made from high strength, case hardened EN-40B nitrided steel. It featured a nitride coating to protect the disk from excessive wear. The mechanical rotor growth was measured as 35 μm at 12,000 rpm and conformed to a linear relation with angular speed.

Compressed air was supplied to the test section at a fixed temperature of 295 K by fourteen 19 mm diameter pipes so that the seal is pressurized asymmetrically, up to a maximum pressure drop of 3.5 bar. A Bronkhorst (Vorden, The Netherlands) F-106CI mass flow meter was installed downstream of the test seal to measure the leakage flow up to a maximum of 0.35 kg/s. A V-721 Brüel & Kjær (Nærum, Denmark) electromagnetic shaker was used to excite the test section. The shaker could supply a maximum load of 3000 N between 10 and 4000 Hz. Displacements of up to 25.4 mm could be created at a maximum of 700 mm/s through a stinger connected to the casing, as shown in Fig. 4. Figure 5 shows the downstream cross-sectional view indicating the locations of the cross-coupled instrumentation and the holes used for balancing the rotor to G2.5 of ISO1940-1:2003.

The direct load was measured using a Novatech (St Leonards on Sea, UK) F317 5 kN load cell, whereas the cross-coupled force was measured using a pair of Omega (Norwalk, CT) LC202 miniature load cells, summed to find the total force applied in the orthogonal plane. Sensonics (Berkhamsted, UK) Senturion PRS02/7.0U01 Eddy current probes (ECPs) were used to measure the displacement in response to the forced vibrations. The load cells and Eddy current probes were used in conjunction to measure the rotordynamic coefficients of the test seals, as described in Sec. 2.3.

2.2 The Seal Designs and Parameters. Two different bristle diameters were studied, termed herein as the "4T" and "5T" (short for four-thousands and five-thousands of an inch) brush seals described in Table 1. Both seals were designed and manufactured in accordance with the in-house protocols of Cross Manufacturing using Haynes 25 for the bristles. They were assembled with a small interference, i, between the bristles tips and the rotor. The casing was centered with respect to the rotor before each experiment took place.

Figure 6 shows the test seal back plate configurations. The front plates of both brush seals have an engine-representative deep bore front plate diameter, which is designed to minimize the disruption of the bristle pack caused by high swirl ratios. The back plate was interchanged between a conventional, flat profile to a pressure-

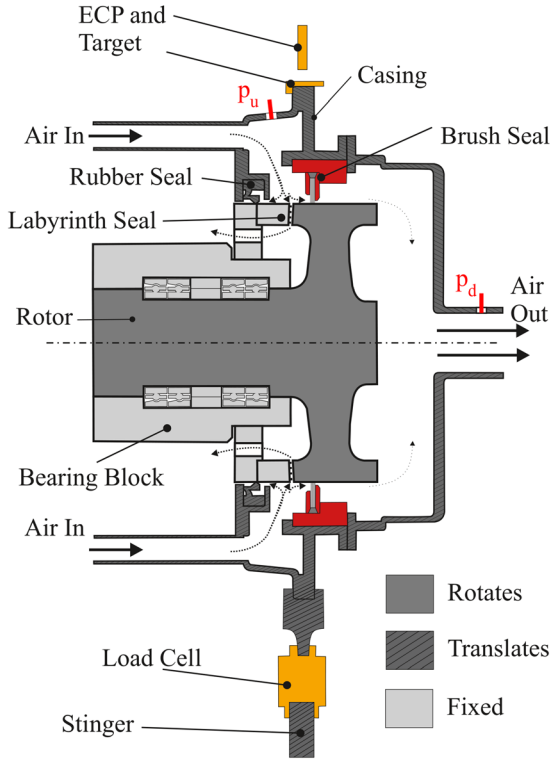

Fig. 4 Cross section view of the dynamic test rig with a brush seal installed

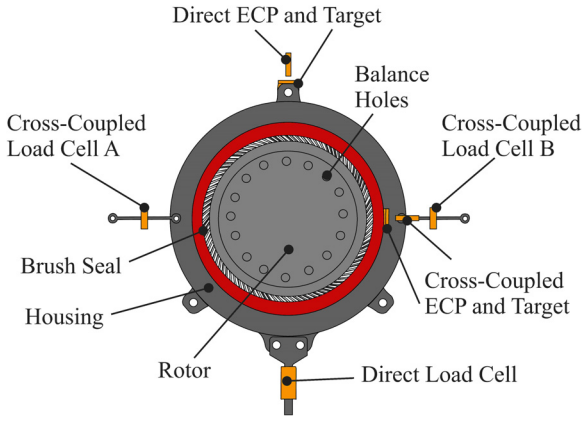

Fig. 5 Downstream cross section view of the dynamic test rig with a brush seal installed

relieved plate with three pockets at different radial positions. The location and radial extent of the pockets are shown in Fig. 6 and are representative of the manufacturer's best practice.

2.3 Rotordynamic Methodology. The method developed by Rouvas and Childs [21] for determining rotordynamic characteristics is used in this study and is summarized herein. A two-dimensional mass–spring–damper system can be described by the following equation:

$$\begin{bmatrix} M_{xx} & M_{xy} \\ M_{yx} & M_{yy} \end{bmatrix} \begin{bmatrix} \ddot{x} \\ \ddot{y} \end{bmatrix} + \begin{bmatrix} C_{xx} & c_{xy} \\ c_{yx} & C_{yy} \end{bmatrix} \begin{bmatrix} \dot{x} \\ \dot{y} \end{bmatrix} + \begin{bmatrix} K_{xx} & k_{xy} \\ k_{yx} & K_{yy} \end{bmatrix} \begin{bmatrix} x \\ y \end{bmatrix} = \begin{bmatrix} f_{ex,x} \\ f_{ex,y} \end{bmatrix} \tag{1}$$

where M is the mass coefficient of the seal, C and K are the direct damping and stiffness coefficients, likewise c and k are the cross-coupled damping and stiffness coefficients, respectively, and f_{ex} is

Table 1 Technical data for the test seals

Parameter	4T	5T
Free bristle height	13.9 mm	
Fence height, h_f	1.88 mm	
Lay angle, θ	45 deg	
Interference, i	0.02 mm	
Pack thickness	1.14 mm	1.37 mm
Bristle diameter	0.102 mm	0.127 mm
	0.004 in	0.005 in
Rows of bristles	11	10
Packing density	78.7 bristles/mm	60.4 bristles/mm

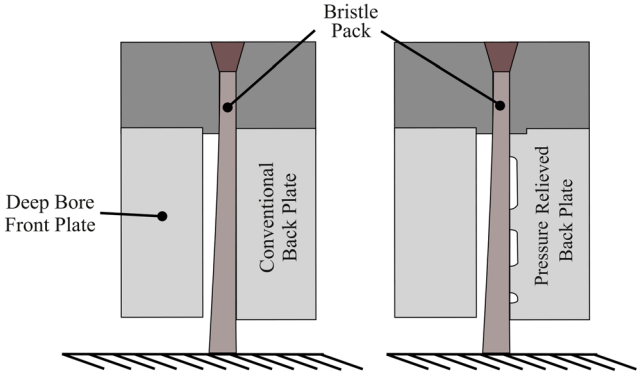

Fig. 6 Conventional and pressure-relieved test configurations

the excitation force. The subscripts describe the direction of the load and where applicable, the second subscript denotes the direction of the response.

Assuming that the excitation force is sinusoidal, and that the subsequent displacement is also sinusoidal, the measured terms may be transformed from the time domain into the frequency domain

$$F_x = \sqrt{\{a_f\}^2 + \{b_f\}^2}\cos(n\omega t - \psi_{f,n}) \tag{2}$$

and

$$X_x = \sqrt{\{a_x\}^2 + \{b_x\}^2}\cos(n\omega t - \psi_{x,n}) \tag{3}$$

where

$$a_f = \frac{1}{2}\int_0^T f(t)\cos(n\omega t)d\tau \tag{4}$$

$$b_f = \frac{1}{2}\int_0^T f(t)\sin(n\omega t)d\tau \tag{5}$$

likewise

$$a_x = \frac{1}{2}\int_0^T x(t)\cos(n\omega t)d\tau \tag{6}$$

$$b_x = \frac{1}{2}\int_0^T x(t)\sin(n\omega t)d\tau \tag{7}$$

Using the same method, the Fourier transforms for the cross-coupled direction may be found. Equation (1) can be rewritten as

$$\begin{bmatrix} H_{xx} & H_{xy} \\ H_{yx} & H_{yy} \end{bmatrix}\begin{Bmatrix} X \\ Y \end{Bmatrix} = \begin{Bmatrix} F_{\mathrm{ex},x} \\ F_{\mathrm{ex},y} \end{Bmatrix} \tag{8}$$

where H_{ij} is the frequency response function (FRF), where each component of the matrix may be described by

$$H_{ij} = K_{ij} - \omega^2 M_{ij} + j\omega C_{ij} \tag{9}$$

Equations (2)–(7) may also be used for a discrete excitation frequency. Therefore, the analysis would be repeated for a range of frequencies to describe the dynamic response of the seal. In this experimental campaign, the system was excited between 15 and 150 Hz in 15 Hz increments. At frequencies above 150 Hz, the signal to noise ratio of the instrumentation was insufficient to ensure the required accuracy for the rotordynamic measurements. Assessment at higher frequencies was therefore beyond the scope of this study.

The real part Eq. (9), $\mathrm{Re}(H_{ij})$, is used to estimate the stiffness and mass coefficients and the imaginary part, $\mathrm{Im}(H_{ij})$, is used to determine the damping coefficients of the seal. A maximum likelihood estimation (MLE) has been used throughout Sec. 4 to calculate these coefficients from the experimental data.

In order to estimate the FRFs in orthogonal directions, the test seal should be excited sequentially in both axes to measure the response in each direction. However, for small amplitudes of oscillation and for an axisymmetric system, it can be assumed that the direct FRFs are equal: $H_{xx} = H_{yy}$, and that the cross-coupled FRFs are equal but opposite: $H_{xy} = -H_{yx}$. As such, the test seal only needs to be excited in one axis to fully characterize the rotordynamic performance.

2.4 Rotordynamic Uncertainty Analysis. In order to minimize any random error, the shaker was used to excite the seal at a given excitation frequency for 10 s. The Fourier analysis described above was conducted on each cycle across the 10 s period, and the average of each $H_{ij}(\omega)$ was found. This was then used to estimate the mass, stiffness, and damping coefficients. Additionally, there will be uncertainty in the measurements from the test facility which subsequently means that each value of $H_{ij}(\omega)$ shown in Eq. (9) at a given excitation frequency is

$$H_{ij}(\omega) = H_{ij}(\omega) \pm e(\omega)_{H_{ij}} \tag{10}$$

where $e_{H_{ij}}$ is the uncertainty from the instrumentation. This can be calculated using the approach outlined by Holman [22]. However, it should also be noted that the uncertainty of H_{ij} in Eq. (10) is frequency-dependent [23,24]. Therefore, $e_{H_{ij}}$ should be derived from the frequency domain using the Fourier transforms of the time-based signals [25]

$$e_{H_{ij}} = \sqrt{\left(\frac{\partial H_{ij}}{\partial F_{ij}}e_{F_{ij}}\right)^2 + \left(\frac{\partial H_{ij}}{\partial X_{ij}}e_{X_{ij}}\right)^2} \tag{11}$$

where $\partial H/\partial F$ and $\partial H/\partial X$ are obtained from the matrix elements of Eq. (8), and the frequency-dependent uncertainties of the instrumentation, e_F and e_X, can be found using the same approach presented in Eqs. (2)–(7).

The instrumentation uncertainty, $\mathrm{Re}(e_{H_{ij}})$ and $\mathrm{Im}(e_{H_{ij}})$ were used to statistically weight the experimental data used in the MLE. This approach has enabled the minimization of the 95th percentile confidence intervals presented in the dynamic coefficient plots, which is a standard method for presenting rotordynamic uncertainty [26,27].

3 Leakage Performance

The dynamic test facility was used to study the leakage performance of the four brush seal configurations. The mass flow data were collected for a range of rotational speeds, pressure differences, and excitation frequencies. Mass flow data presented hereafter represent averages of steady-state conditions over a 10 s period, with each dataset repeated three times to ensure reliability. The leakage of the 4T conventional seal is presented in Fig. 7. This was measured for a range of pressure drops at five different

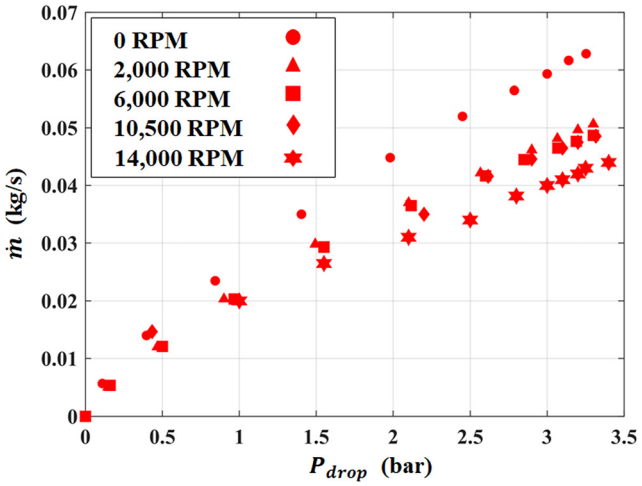

Fig. 7 Leakage through the 4T conventional seal with pressure difference at varied rotational speeds

rotational speeds. The experimental mass flow decreased with increasing rotational speed, in line with previous findings [11,12]. The reduction in mass flow is due to the combined effect of the reduced clearance with rotor growth and the increased length of the leakage pathway through the brush seal with increasing tangential velocity [1]. The change in gradient at a pressure ratio $(p_u/p_d) = 1.9$ is indicative of the critical pressure ratio for an orifice and signifies the air passing through the seal is choked.

The 4T bristle pack with pressure-relieved back plate and the 5T conventional and pressure-relieved seal were tested in the same manner. In order to compare different seal configurations, the effective clearance, s_{eff}, is regularly used to evaluate leakage characteristics [4]. This dimensional parameter is equivalent to an annular restriction of the same diameter as the tested seal required to pass the measured leakage isentropically [19]

$$s_{\text{eff}} = \frac{\dot{m}\sqrt{T}}{\pi D p_u Q} \tag{12}$$

where

$$Q = \sqrt{\frac{2\gamma}{R(\gamma-1)}\left\{\left(\frac{p_u}{p_d}\right)^{-\frac{2}{\gamma}} - \left(\frac{p_u}{p_d}\right)^{-\frac{\gamma+1}{\gamma}}\right\}} \quad \text{for} \quad \left(\frac{p_u}{p_d}\right) < \left(\frac{2}{\gamma+1}\right)^{-\frac{\gamma}{\gamma-1}}$$
$$= \sqrt{\frac{\gamma}{R}\left\{\frac{2}{\gamma+1}\right\}^{\frac{\gamma+1}{\gamma-1}}} \quad \text{for} \quad \left(\frac{p_u}{p_d}\right) > \left(\frac{2}{\gamma+1}\right)^{-\frac{\gamma}{\gamma-1}} \tag{13}$$

Figure 8 shows the effective clearance of the 5T seal with different back plates. As above, at pressure drops greater than 0.9 the flow is choked and the effective clearance tends toward a plateau. The conventional brush seal shows a distinct reduction in effective clearance with between 0 and 2000 rpm, but little further reduction at higher speeds. The pressure-relieved pockets increased the leakage, and therefore the effective clearance, compared to the conventional back plate for all rotational speeds considered. The change in leakage with rotation was more pronounced for the pressure-relieved brush seal.

Figure 9 compares the effective clearance of the four configurations of brush seal without rotation. Increased bristle diameter gives rise to an increase in leakage flow and in turn the effective clearance of the brush seal. This was expected as the increase in bristle diameter results in a smaller packing density, shown in Table 1, which leads to a larger area for the fluid to pass through. Additionally, the pressure-relieved back plate caused an increase in effective clearance for both bristle packs. The use of

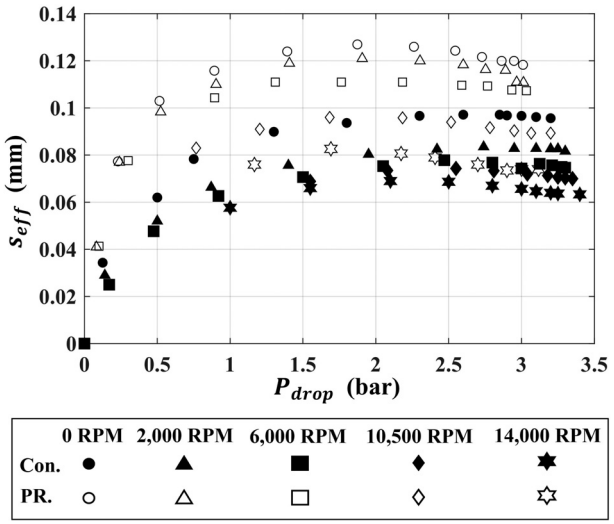

Fig. 8 Effective clearance of the 5T conventional seal (Con.) and pressure-relieved (PR.) with pressure

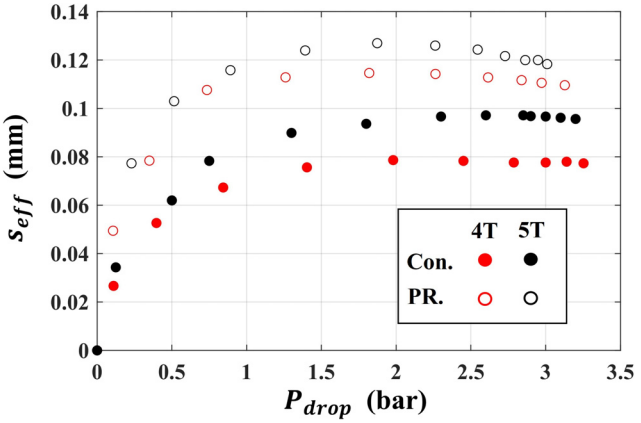

Fig. 9 Effective clearance of the 4T and 5T conventional (Con.) and pressure-relieved (PR.) seals without shaft rotation

pressure-relieved pockets corresponds to a decrease in compression and an increase in radial mass flow, increasing the leakage through the pack.

The mass flow is shown to be invariant with frequency and time when excited. For example, Figs. 10(*a*) and 10(*b*) show the measured mass flow of the 5T seal with a conventional back plate at 15 Hz and 150 Hz excitation frequency, respectively. For small excitation amplitudes, the bristles will compress in response to the excitation on one side of the seal and open at the opposite side of the rotor. It is therefore possible that the increase in local leakage at one side will be canceled out by a reduction through the compressed bristles on the other side so the total resistance to the flow is conserved. However, as the mass flowmeter is positioned significantly downstream of the bristle pack, any time-resolved fluctuations in mass flow are also likely to be damped out before reaching the measurement location. Nevertheless, the engine designer is primarily interested in the time averaged mass flowrate, which is unaffected by excitation frequency over the range tested in this study.

4 Rotordynamic Measurements

This section presents an example FRF and describes the processes required to estimate the direct rotordynamic coefficients of a brush seal subject to pressure and rotation. The stiffness and damping coefficients for the four seal configurations are then presented and discussed.

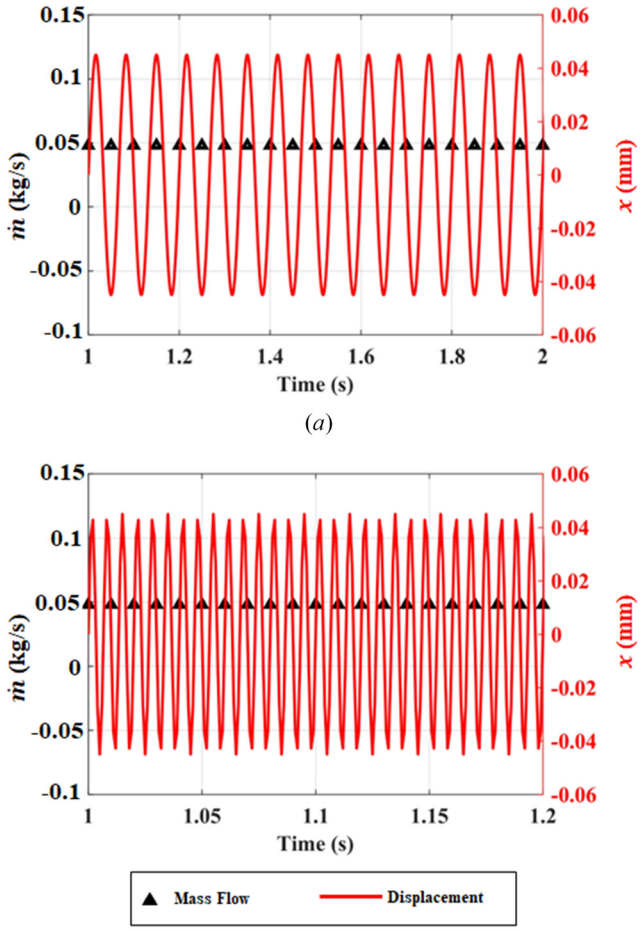

Fig. 10 Mass flow and displacement of the 5T brush seal at 1.9 bar and 2000 rpm, excited at 15 Hz (*a*) and 150 Hz (*b*)

4.1 A Frequency Response Example. The rotordynamic methodology introduced in Sec. 2.3 is used in the following example for the 4T brush seal at a pressure drop of 2 bar and a shaft speed of 4000 rpm.

It is important to note that the test facility will have associated FRFs (H_r). In other words, the rig has its own characteristic mass, stiffness, and damping coefficients which need to be considered. The test section was excited using the electromagnetic shaker for 10 s at a given frequency. This was repeated for ten individual frequencies, 15–150 Hz in 15 Hz increments to produce the complete FRF. The measured load and displacements were transformed to the frequency domain using Eqs. (2)–(7).

The seal was then installed and the process was repeated in order to find the combined seal and test rig FRFs (H_{rs}), and the difference between H_r and H_{rs} can be used to approximate the FRF of the mechanical components of brush seal, H_s. The difference between $\text{Re}(H_{\text{rs}})$ and $\text{Re}(H_r)$ yields $\text{Re}(H_s)$, which can be used to find the stiffness and mass coefficients for the seal without pressure or rotational effects. Likewise, the imaginary parts, $\text{Im}(H_{\text{rs}})$ and $\text{Im}(H_r)$ give $\text{Im}(H_s)$, which can be used to find the damping response. This is described analytically by

$$\begin{aligned} \text{Re}(H_s) &= \text{Re}(H_{\text{rs}}) - \text{Re}(H_r) \\ \text{Im}(H_s) &= \text{Im}(H_{\text{rs}}) - \text{Im}(H_r) \end{aligned} \tag{14}$$

The mechanical rotordynamic components of the brush seal will affect all subsequent pressurization tests, with and without rotation. To account for day-to-day variation, the installed seal was shaken without pressure and rotation at the beginning of a test campaign to find the baseline FRF (H_b). Upstream pressure was applied and rotational speed increased until the desired test conditions were reached. The electromagnetic shaker was then used to excite the pressurized system and the load and displacement were measured. The difference between the total response (H_t) and baseline test isolates the effects of pressurization and rotation (H_p), as described by

$$\begin{aligned} \text{Re}(H_p) &= \text{Re}(H_t) - \text{Re}(H_b) \\ \text{Im}(H_p) &= \text{Im}(H_t) - \text{Im}(H_b) \end{aligned} \tag{15}$$

However, this also removes the bristle stiffness and damping properties of the seal. Therefore the isolated mechanical response (H_s) found using Eq. (14) is added to the pressurized response (H_p) found from Eq. (15) to describe the FRFs of the pressurized system

$$\begin{aligned} \text{Re}(H_{ps}) &= \text{Re}(H_p) + \text{Re}(H_s) \\ \text{Im}(H_{ps}) &= \text{Im}(H_p) + \text{Im}(H_s) \end{aligned} \tag{16}$$

This process is represented in Fig. 11. The MLE fits of the real and imaginary parts yield the stiffness, mass, and frequency-dependent damping coefficients for the pressurized system subject to rotation. Error bars are included for all data points, calculated in accordance with the method outlined in Sec. 2.4. In most cases, the error bars are smaller than the data point symbols.

Figure 11(*a*) shows that when subject to 2 bar pressure drop and 4000 rpm shaft speed, the brush seal has a stiffness and mass coefficient of 4100 kN/m and 9.42 kg, respectively. The total mass of the brush seal components indicated in red in Fig. 4 was 9.85 kg, demonstrating that the mass coefficient of the system is equal to the mass of the test seal within the error of the response. Figure 11

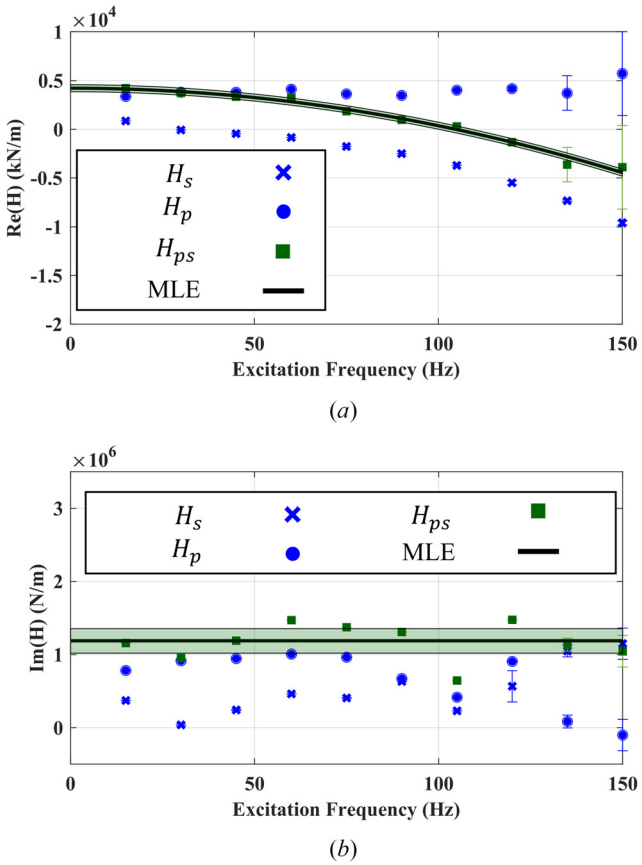

Fig. 11 The real (*a*) and imaginary (*b*) parts of the FRFs of the test facility with a brush seal subject to pressure and rotation summed with the mechanical FRFs to find the dynamic coefficients

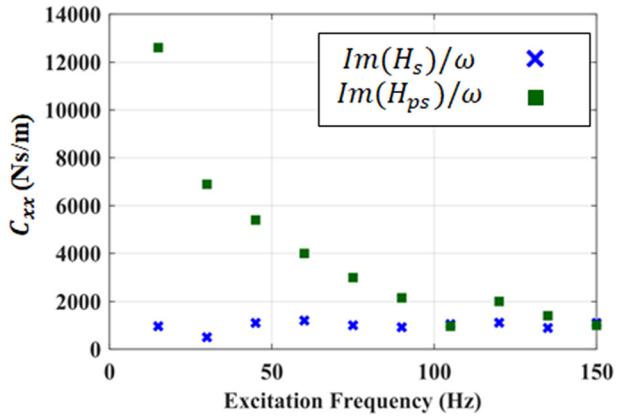

Fig. 12 Direct damping coefficient of the pressurized seal reduces with increasing excitation frequency, whereas the unpressurized seal is invariant

further shows that the pressure-only response offers no added mass to the system and that the total mass coefficient is caused only by the mechanical response.

Figure 11(*b*) shows that the MLE fit to the data for the pressurized seal may be represented as a constant value. This demonstrates that the seal behaves as a Coulomb damper when subject to pressure. Hence, the equivalent viscous damping coefficient decreases with excitation frequency

$$C = \frac{\mathrm{Im}(H)}{\omega} \tag{17}$$

Conversely, without pressure or rotation, the isolated mechanical seal behaves as a viscous damper, where $\mathrm{Im}(H_s)$ increases linearly with excitation frequency. In other words, Eq. (17) yields a damping coefficient that is independent of frequency, as shown by the $\mathrm{Im}(H_s)/\omega$ values in Fig. 12. Increasing the excitation frequency of the pressurized seal, $\mathrm{Im}(H_{\mathrm{ps}})/\omega$, caused the damping coefficient to tend toward the mechanical value, $\mathrm{Im}(H_s)/\omega$, of approximately 1000 Ns/m.

4.2 The Influence of Pressure and Back Plate Design on Dynamic Characteristics. The direct stiffness and damping coefficients of the 4T brush seal with a conventional back plate are shown in Figs. 13 and 14, respectively. The cross-coupled stiffness is presented in Fig. 15. As described in Sec. 4.1, the mechanical stiffness and damping of the seal were initially tested in the absence of pressure and rotation. Three different pressure drops, 1, 2, and 3 bar were then applied and the rotational speed increased.

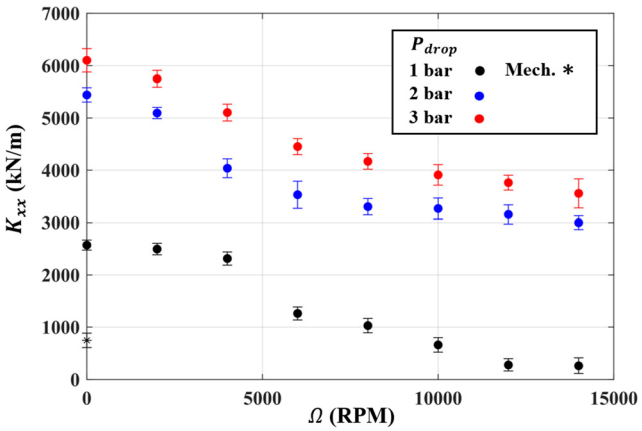

Fig. 13 Direct stiffness of the 4T brush seal with conventional back plate at different pressure drops and rotational speeds

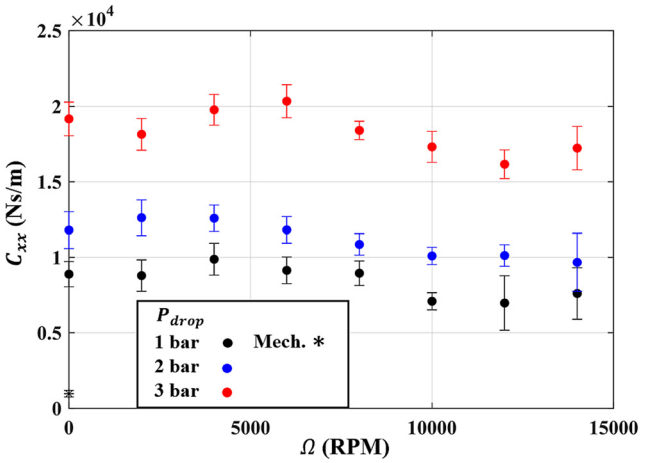

Fig. 14 Direct damping of the 4T brush seal with conventional back plate at different pressure drops and rotational speeds at an excitation frequency of 15 Hz

Figures 13 and 14 show an increase in the rotordynamic coefficients as pressure drop is increased. Figure 13 shows a decrease in the stiffness of the seal that plateaus at higher rotational speeds. Figure 14 shows that the direct damping increases with pressure drop, but that rotational speed has a limited impact on the coefficients. Data were collected for the full range of tested excitation frequencies, however, as the trends were qualitatively similar, example results are only presented here for an excitation frequency of 15 Hz.

Figure 15 shows that the cross-coupled stiffness coefficient is very small compared with the direct coefficients and largely within the uncertainty of the cross-coupled FRF. Additionally, there is no meaningful trend with rotational speed or pressure difference and the pressurized response is comparable with the mechanical stiffness. Further scrutiny of these data found this was caused by the minimal displacement in the cross-coupled direction. This is attributed to the fact the bristle pack rests on the rotor, and therefore any residual movement in the cross-coupled plane would be resisted by these points of contact.

In other words, the bristles would hold the rotor in place relative to any movement. Notably, this cross-coupled response was found across all four brush seal configurations.

Figure 16 shows that the pressure-relieved back plate minimized the impact of rotational speed on the stiffness coefficient. In the case of the conventional configuration, stiffness approached the same value as the pressure-relieved seal as rotational speed increased.

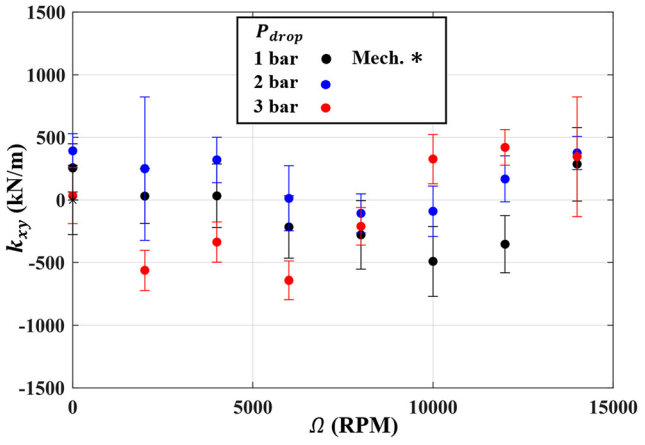

Fig. 15 Cross-coupled stiffness of the 4T brush seal with conventional back plate at different pressure drops and rotational speeds

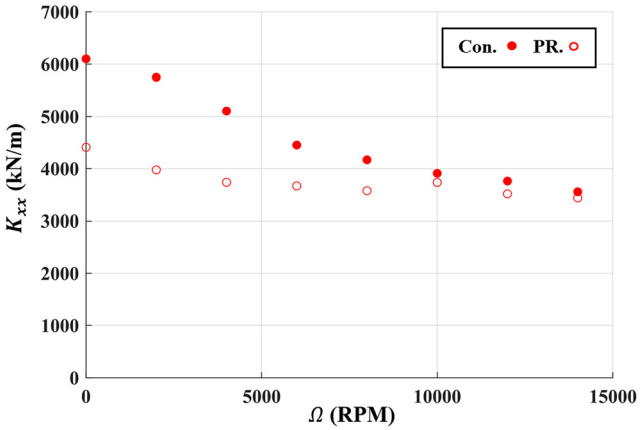

Fig. 16 Direct stiffness of the 4T brush seal at 3 bar pressure difference with a conventional and a pressure-relieved back plate with rotational speed

Figure 17 shows that the damping coefficients of both configurations are invariant with shaft speed; however, the pressure-relieved seal is approximately half as damped as the conventional seal. The change in dynamic behavior between the back plate configurations is attributed to the purpose of the pressure-relieving pockets to reduce the friction between the bristle pack and the back plate. Reduced hysteresis and bind-up will minimize the impact of rotation on the stiffness of the seal, and reduced friction will decrease the damping of the bristle pack.

Although not directly presented here, an increase in the dynamic coefficients with pressure was also found for the 5T seal. The pressure-relieved back plate reduced the impact of rotational speed on the stiffness coefficient and reduced the damping coefficient for all speeds, as indicated in Figs. 18 and 19, respectively.

The reduction in stiffness and invariance in damping coefficients with rotational speed for the conventional seals is similar to the findings of Conner and Childs [13], who speculate that the reduction in stiffness may be due to the bristles lifting from the rotor, with a fluid film developing underneath the tips. However, the pressure-relieved back plate reduced the impact of rotational speed on seal stiffness. This is contrary to the leakage behavior shown in Fig. 8, where changes with rotational speed were less pronounced for the conventional seal.

4.3 The Influence of Bristle Diameter on Dynamic Characteristics. The dynamic characteristics of the 4T and 5T seals can be compared to study the impact of bristle diameter and packing density. Figures 16 and 18 show the 5T seal was stiffer than the 4T seal, irrespective of the back plate configuration. Comparing Figs. 17 and 19 show that the 5T seal was less damped than the 4T seal when subject to the same conditions.

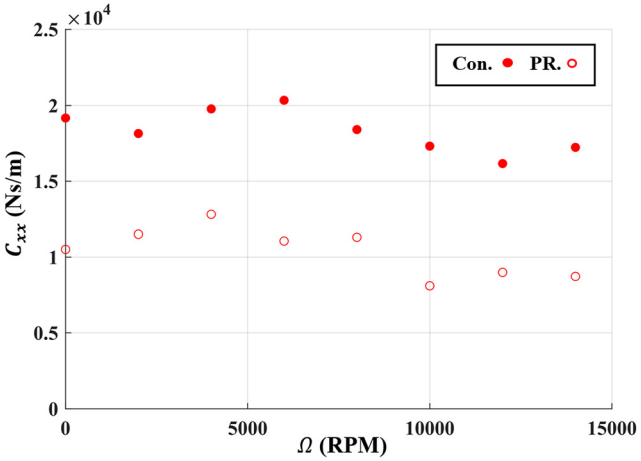

Fig. 17 Direct damping at an excitation frequency of 15 Hz of the 4T brush seal at a 3 bar pressure difference with conventional and a pressure-relieved back plate with rotational speed

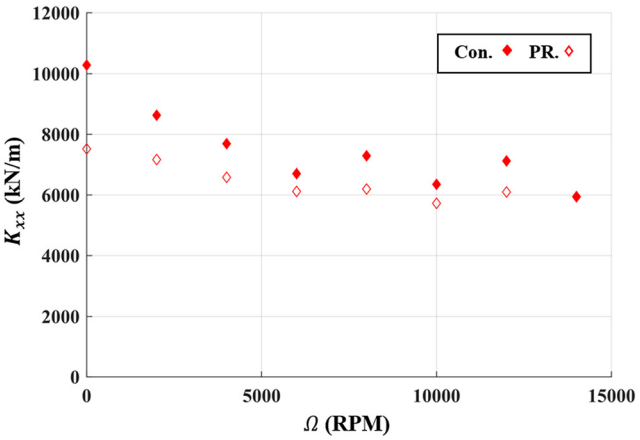

Fig. 18 Direct stiffness of the 5T brush seal at a 3 bar pressure difference with a conventional and a pressure-relieved back plate with rotational speed

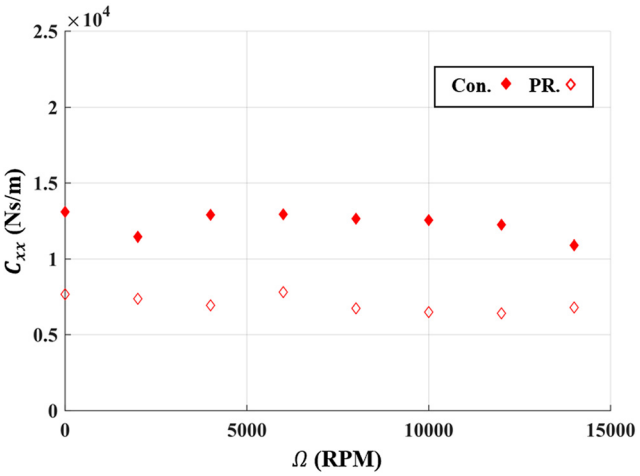

Fig. 19 Direct damping at an excitation frequency of 15 Hz of the 5T brush seal at a 3 bar pressure difference with conventional and a pressure-relieved back plate with rotational speed

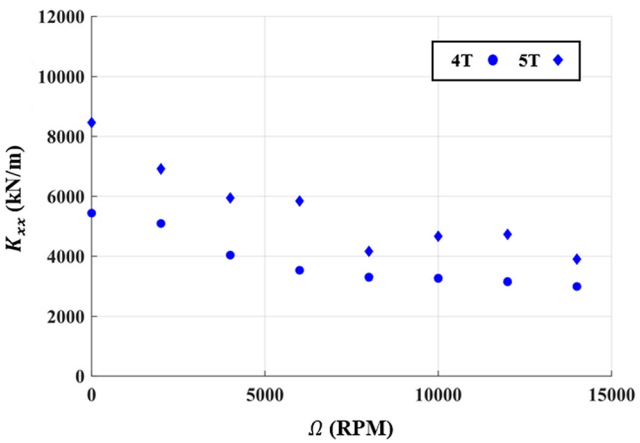

Fig. 20 Direct stiffness of the 4T and 5T brush seals with a conventional back plate at 2 bar pressure difference

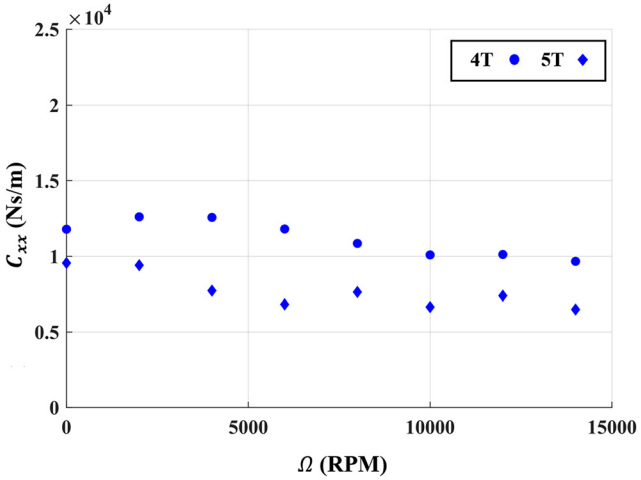

Fig. 21 Direct damping at an excitation frequency of 15 Hz of the 4T and 5T brush seals with a conventional back plate at 2 bar pressure difference

The trends between the two bristle diameters were consistent at different pressure drops. For example, Figs. 20 and 21 compare the dynamic coefficients of the conventional 4T and 5T brush seals at 2 bar pressure difference. Figure 20 shows that the 5T brush seal was stiffer than the 4T seal for the full range of rotational speeds. Figure 21 shows that the 4T seal had a larger damping coefficient for the same operational conditions compared with the 5T bristle pack.

The increased stiffness of the 5T seals is attributed to the greater second moment of area of the bristle. The decrease in damping coefficient may be understood by considering the packing density of the two bristle packs. The 4T seal has a packing density of 78.7 bristles/mm, whereas the 5T seal is 60.4 bristles/mm. As there are fewer bristle-to-bristle interactions, there is less interbristle friction within the pack and therefore less resistance to excitation.

5 Conclusions

This study presents rotordynamic and leakage characteristics of a single-stage brush seal tested in isolation. Four seals were manufactured from the latest in seal material technology with modern design practices. They featured two different bristle diameters and pack densities, as well as two back plate designs. The tests took place over a wide range of conditions, including pressure ratios of up to 4.5, rotational speeds up to 14,000 rpm, and excitation frequencies up to 150 Hz.

The seal leakage was shown to increase with bristle diameter due to the increased spacing between the bristles reducing the resistance to the flow. The use of a pressure-relieved back plate also increased leakage compared to a conventional flat back plate for both seals when installed with a slight interference. It was found that increasing the rotational speed of the dynamic test rig reduced the leakage flow for all seals. This was due to a combined effect of the increased flow path length caused by the tangential direction of the flow, as well as rotor growth reducing the clearance of the seal.

The direct stiffness and damping coefficients for all brush seals tested were found to increase with pressure difference. The seals with a conventional back plate were found to have a direct stiffness coefficient that reduced with rotational speed before plateauing at higher speeds. On the other hand, rotational speed was found to have a limited effect on the damping coefficients of the seals. The stiffness coefficients for the pressure-relieved seals were reduced at low rotational speeds. However, at higher speeds, the stiffness converged toward the values for the conventional back plate design. The effect of the pressure-relieved back plate was to reduce the damping coefficients for both bristle diameters tested.

Increasing the bristle diameter was found to increase the stiffness coefficient of the seal, which was attributed to the increase in the second moment of area of the individual bristles. Conversely, the damping coefficient was found to decrease with bristle diameter due to the reduction in packing density.

Acknowledgment

The authors are extremely grateful for the technical support of Andrew Langley, Jim Cansell, and Qian Li who enabled the use of the test facility. Cross Manufacturing is thanked for funding this study.

Funding Data

- Engineering and Physical Sciences Research Council (Award No. EP/P008232/1; Funder ID: 10.13039/501100000266).

Data Availability Statement

The datasets generated and supporting the findings of this article are obtainable from the corresponding author upon reasonable request.

Nomenclature

a = Fourier coefficient
b = Fourier coefficient
c = cross-coupled damping coefficient (Ns/m)
C = direct damping coefficient (Ns/m)
D = rotor diameter (m)
e = error
f = load (N)
F = Fourier transformed load (N)
H = complex stiffness (N/m)
h_f = fence height (m)
h_{fb} = free bristle height (m)
i = bristle interference (m)
k = cross-coupled stiffness coefficient (N/m)
K = direct stiffness coefficient (N/m)
M = mass coefficient (kg)
$\dot{m}$ = mass flow (kg/s)
n = cycle number
p = pressure (bar or N/m^2)
Q = pressure ratio dependent parameter (K$^{1/2}$s/m)
R = gas constant (J/kg K)
s = clearance (m)
t = time (s)
T = measured temperature (K)
x = measured displacement (m)
X = Fourier transformed displacement in x (m)
y = measured displacement (m)
Y = Fourier transformed displacement in y (m)
γ = heat capacity ratio
θ = lay angle (deg)
ψ = phase angle (rad/s)
ω = excitation frequency (rad/s or Hz)

Superscripts and Subscripts

b = baseline
d = downstream value
eff = effective parameter
ex = excitation
f = load parameter
i, j = general complex stiffness coordinates
p = pressure only response
ps = pressurized seal response
r = rig only
rs = rig with seal installed
s = seal parameter only
t = total response

u = upstream value
x = in x direction
y = in y direction
$\dot{}$ = first derivative (/s)
$\ddot{}$ = second derivative (/s^2)

References

[1] Bowen, J., Bird, J., Cross, H., Jenkins, M., Bowsher, A., Crudgington, P., Sangan, C., and Scobie, J., 2024, "Fluid Dynamic Behaviour of Conventional and Pressure Relieving Brush Seals," ASME J. Eng. Gas Turbines Power, **146**(6), p. 061001.
[2] Thomas, H., 1958, "Unstable Oscillations of Turbine Rotors Due to Steam Leakage in the Clearance of the Sealing Glands and the Buckets," Bull. Sci. AJM, **71**, pp. 1039–1063.
[3] Alford, J., 1964, "Protection of Labyrinth Seals From Flexural Vibration," ASME J. Eng. Gas Turbines Power, **86**(2), pp. 141–147.
[4] Chupp, R., Hendricks, R., Lattime, S., and Steinetz, B., 2006, "Sealing in Turbomachinery," J. Propul. Power, **22**(2), pp. 313–349.
[5] Bird, J., Keogh, P., Sangan, C., Bowsher, A., Crudgington, P., and Scobie, J., 2024, "Dynamic Characterization of an Adaptive Film-Riding Seal," ASME J. Eng. Gas Turbines Power, **146**(1), p. 011017.
[6] Ferguson, J., 1988, "Brushes as High Performance Gas Turbine Seals," ASME Paper No. 88-GT-182.
[7] Dinc, S., Demiroglu, M., Turnquist, N., Mortzheim, J., Goetze, G., Maupin, J., Hopkins, J., Wolfe, C., and Florin, M., 2002, "Fundamental Design Issues of Brush Seals for Industrial Applications," ASME J. Turbomach., **124**(2), pp. 293–300.
[8] Kirk, T., Bowsher, A., Crudgington, P., and Chupp, R., 2015, "Aspects of Brush Seal Design," AIAA Paper No. 2015-4230.
[9] Chen, L., 1998, "Numerical and Experimental Modelling of Brush Seals," D.Phil thesis, University of Oxford, Oxford, UK.
[10] Hendricks, R., Griffin, T., Kline, T., Csavina, K., Pancholi, A., and Sood, D., 1994, "Relative Performance Comparison Between Baseline Labyrinth and Dual Brush Compressor Discharge Seals in a T-700 Engine Test," ASME Paper No. 94-GT-266.
[11] Pekris, M., Franceschini, G., and Gillespie, D., 2014, "An Investigation of Flow, Mechanical, and Thermal Performance of Conventional and Pressure-Balanced Brush Seals," ASME J. Eng. Gas Turbines Power, **136**(6), p. 062502.
[12] Proctor, M., and Delgado, R., 2004, "Leakage and Power Loss Test Results for Competing Turbine Engine Seals," ASME Paper No. GT2004-53935.
[13] Conner, K., and Childs, D., 1993, "Rotordynamic Coefficient Test Results for a Four-Stage Brush Seal," J. Propul. Power, **9**(3), pp. 462–465.
[14] Gaszner, M., Pugachev, A. O., Georgakis, C., and Cooper, P., 2013, "Leakage and Rotordynamic Coefficients of Brush Seals With Zero Cold Clearance Used in an Arrangement With Labyrinth Fins," ASME J. Eng. Gas Turbines Power, **135**(12), p. 122506.
[15] Pugachev, A., and Deckner, M., 2012, "Experimental and Theoretical Rotordynamic Stiffness Coefficients for a Three-Stage Brush Seal," Mech. Syst. Signal Process., **31**, pp. 143–154.
[16] Ha, Y., Ha, T., Byun, J., and Lee, Y., 2020, "Leakage Effects Due to Bristle Deflection and Wear in Hybrid Brush Seal of High-Pressure Steam Turbine," Tribol. Int., **150**, p. 106325.
[17] Delgado, A., San Andrés, L., and Justak, J., 2005, "Measurements of Leakage, Structural Stiffness and Energy Dissipation Parameters in a Shoed Brush Seal," Sealing Technol., **2005**(12), pp. 7–10.
[18] Delgado, A., San Andrés, L., and Justak, J., 2004, "Analysis of Performance and Rotordynamic Force Coefficients of Brush Seals With Reverse Rotation Ability," ASME Paper No. GT2004-53614.
[19] Pedraza-Valle, E., Scobie, J., Sangan, C., Keogh, P., Bowsher, A., and Crudgington, P., 2019, "A New Rotating Test Facility for the Experimental Characterisation of Shaft Seals," Proceedings of the 13th European Conference on Turbomachinery Fluid Dynamics and Thermodynamics, Lausanne, Switzerland, Apr. 8–12, pp. 1–11.
[20] Bird, J., 2023, "The Development of Novel Shaft Seals for Turbomachinery," Ph.D. thesis, University of Bath, Bath, UK.
[21] Rouvas, C., and Childs, D., 1993, "A Parameter Identification Method for the Rotordynamic Coefficients of a High Reynolds Number Hydrostatic Bearing," ASME J. Vib. Acoust., **115**(3), pp. 264–270.
[22] Holman, J., 2021, *Experimental Methods for Engineers*, 8th ed., McGraw-Hill, Boston, MA.
[23] Medina, L., Ruiz, R., and Díaz, S., 2008, "A Simple Approach to Determine Uncertainty Bounds on Bearing Rotordynamic Coefficients Identification," ASME Paper No. GT2008-51200.
[24] Liguori, C., 2001, "Uncertainty on Signal Parameter Estimation in Frequency Domain," Proceedings of the 11th IMEKO TC-4, Lisbon, Portugal, Sept. 13–14, pp. 276–280.
[25] Griebel, C., 2021, "Rotordynamic Behavior of Leaf Seals: Measurement of Frequency-Dependent Force Coefficients for Varying Inlet Parameters," ASME J. Eng. Gas Turbines Power, **143**, p. 061002.
[26] AIAA, 1995, "Assessment of Wind Tunnel Data Uncertainty," AIAA Standard No. S-071-1995.
[27] Matta, P., and Arghir, M., 2012, "Identification Method for Rotordynamic Coefficients of Cylindrical Air Bearing Using an Impact Hammer," Proc. Inst. Mech. Eng., Part J, **226**(3), pp. 199–212.